



Susorney, H. C. M., Barnouin, O. S., Ernst, C. M., & Stickle, A. M. (2018). The Surface Roughness of Large Craters on Mercury. *Journal of Geophysical Research: Planets*, 123(7), 1581-1595.  
<https://doi.org/10.1029/2017JE005462>

Peer reviewed version

Link to published version (if available):  
[10.1029/2017JE005462](https://doi.org/10.1029/2017JE005462)

[Link to publication record in Explore Bristol Research](#)  
PDF-document

This is the author accepted manuscript (AAM). The final published version (version of record) is available online via Wiley at <https://agupubs.onlinelibrary.wiley.com/doi/full/10.1029/2017JE005462> . Please refer to any applicable terms of use of the publisher.

## **University of Bristol - Explore Bristol Research**

### **General rights**

This document is made available in accordance with publisher policies. Please cite only the published version using the reference above. Full terms of use are available:  
<http://www.bristol.ac.uk/pure/about/ebr-terms>

# 1 **The Surface Roughness of Large Craters on Mercury**

Hannah C. M. Susorney,<sup>1,2</sup> Olivier S. Barnouin,<sup>3,4</sup> Carolyn M. Ernst,<sup>3</sup> and

Angela M. Stickle<sup>3</sup>

---

Corresponding author: H. C. M. Susorney, Department of Earth, Atmospheric and Ocean Sciences, University of British Columbia, Vancouver, B.C., V6T 1Z4, Canada (hsusorney@eoas.ubc.ca)

<sup>1</sup>Department of Earth and Planetary

**Key Points.**

- For horizontal scales less than 10km, ejecta related processes drive surface roughness around large craters
- Surface roughness at scales of 0.5–250 km are not correlated with crater density (diameters of 20-120 km).

**Abstract.** This study investigates how individual large craters on Mercury (diameters of 25–200 km) can produce surface roughness over a range of baselines (the spatial horizontal scale) from 0.5 ? 250 km. Surface roughness is a statistical measure of change in surface height over a baseline after topography has been detrended. We use root-mean-square (RMS) devi-

---

Science, The Johns Hopkins University,  
Baltimore, MD 21218, USA.

<sup>2</sup>Department of Earth, Ocean and  
Atmospheric Sciences, University of British  
Columbia, Vancouver, BC V6T 1Z4,  
Canada

<sup>3</sup>The Johns Hopkins University Applied  
Physics Laboratory, Laurel, MD 20723,  
USA.

<sup>4</sup>Hopkins Extreme Material Institute, The  
Johns Hopkins University, Baltimore, MD  
21218, USA.

7 ation as our measure of surface roughness. Observations of large craters on  
8 Mercury at baselines from 0.5-10 km found higher surface roughness values  
9 at the central uplifts, rims, and exteriors of craters, while the crater floors  
10 exhibit the lowest roughness values. At baselines less than 10 km, the regions  
11 exterior to large craters with diameters  $> 80$  km have the highest surface  
12 roughness values. These regions, which include the ejecta and secondary fields,  
13 are the main contributors to the increased surface roughness observed in high-  
14 crater-density regions. For baselines larger than 10 km, the crater cavity it-  
15 self is the main contributor to surface roughness. A suite of numerical inves-  
16 tigation used the measured surface roughness obtained in the study to model  
17 the cumulative effect of adding large craters to a surface. The results indi-  
18 cate that not all of the surface roughness on Mercury is due to fresh large  
19 craters, but that impact craters likely contribute to the Hurst exponent from  
20 baselines of 0.5 – 1.5 km and the shape of the deviogram. The simulations  
21 show that a surface becomes reaches a steady-state in surface roughness at  
22 these baselines studied well before the surface was covered in impact craters.

## 1. Introduction

23 Impact craters modify the topography of planetary surfaces. We can quantify the  
24 influence of impact craters on the topography of a planetary surface through a statistical  
25 measure of the change in detrended vertical topography over a given horizontal scale,  
26 surface roughness [e.g., *Shepard et al.*, 2001]. Previous studies have shown that impact  
27 craters increase measured surface roughness values [e.g., *Kreslavsky et al.*, 2008; *Rosenburg*  
28 *et al.*, 2011; *Pommerol et al.*, 2012; *Kreslavsky et al.*, 2013; *Yokota et al.*, 2014; *Kreslavsky*  
29 *et al.*, 2014; *Rosenburg et al.*, 2015; *Fa et al.*, 2016; *Kreslavsky and Head*, 2016; *Susorney*  
30 *et al.*, 2017], in this study we focus on investigating how surface roughness characteristics  
31 can reflect the physical attributes of an individual impact crater (e.g., the crater floor,  
32 ejecta, secondary cratering field) and use a numerical investigation to explore how the  
33 regional surface roughness of Mercury is related to large craters (diameters from 25–200  
34 km).

35 Prior investigations of surface roughness on the Moon and Mercury using many dif-  
36 ferent measures of surface roughness found correlations between regions of high surface  
37 roughness values and regions with high crater density [*Kreslavsky et al.*, 2008; *Rosenburg*  
38 *et al.*, 2011; *Pommerol et al.*, 2012; *Kreslavsky et al.*, 2013; *Yokota et al.*, 2014; *Kreslavsky*  
39 *et al.*, 2014; *Rosenburg et al.*, 2015; *Fa et al.*, 2016; *Kreslavsky and Head*, 2016; *Susor-*  
40 *ney et al.*, 2017] regardless of the measure used. An implicit assumption in interpreting  
41 the apparent correlation between crater density and surface roughness is that the crater  
42 cavities (the primary topographic depression) are the main factors increasing the mea-  
43 sured surface roughness. This assumption has led several authors [e.g., *Rosenburg et al.*,

44 2011; *Yokota et al.*, 2014; *Fa et al.*, 2016] to propose that surface roughness could be used  
45 as a complementary method to crater counts [e.g., *Group*, 1979] to estimate the age of  
46 planetary surfaces.

47 Two studies [*Yokota et al.*, 2014; *Rosenburg et al.*, 2015] investigated in greater detail  
48 the relationship between crater density and surface roughness. *Yokota et al.* [2014] mea-  
49 sured the surface roughness of the Moon using the measure of median differential slope  
50 [*Kreslavsky and Head*, 2000] at horizontal baselines ( $L$ ) of 0.15-100 km. The study found  
51 that the median differential slope at  $L = 20$  km correlated well with the cumulative den-  
52 sity of craters ( $N$ ) with diameters greater than 20 km [ $N(> 20)$ ]. A second correlation  
53 with  $N(> 20)$  was found at  $L = 6-9$  km. The study also used simulated topography with  
54 craters modeled as modified cones to test whether they could reproduce the correlation of  
55 surface roughness with crater density. The correlation at  $L = 20$  km was reproduced, but  
56 the simulated topography did not reproduce the correlation at  $L = 6-9$  km. The difference  
57 at the smaller baselines (6-9 km) was attributed to the fact that secondary craters and  
58 details of ejecta deposits were not incorporated into the model.

59 *Rosenburg et al.* [2015] investigated how idealized crater morphology affected topo-  
60 graphic power spectral density on the Moon with a simplified model of crater morphology,  
61 but did not directly focus on the relationship between crater density and age. The study  
62 found the simulated power spectral slope was dependent on the production function of  
63 impact craters. The model successfully reproduced the measured power spectra of the  
64 lunar surface at baselines of 0.115-1 km.

65 Several studies have discussed the increase in surface roughness associated with individ-  
66 ual impact craters as part of a roughness assessment for broader regions across Mercury

67 [*Harmon et al.*, 2007; *Neish et al.*, 2013; *Kreslavsky et al.*, 2014; *Fa et al.*, 2016; *Su-*  
68 *sorney et al.*, 2017]. The centimeter-scale surface roughness of Mercury’s craters was  
69 approximated using Arecibo radar [*Harmon et al.*, 2007] and an increase in radar bright-  
70 ness (corresponding to higher surface roughness values) was associated with a few large  
71 craters (e.g., the crater Hokusai). The centimeter-scale radar brightness was later at-  
72 tributed to large volumes of impact melt in and around craters on Mercury [*Neish et al.*,  
73 2013]. More recent studies of Mercury’s surface roughness at baselines comparable to the  
74 above-mentioned lunar studies used a range of different surface roughness measurements  
75 [*Fa et al.*, 2016; *Kreslavsky et al.*, 2014; *Susorney et al.*, 2017] and data from the MEr-  
76 cury Surface, Space ENvironment, GEochemistry, and Ranging (MESSENGER) mission.  
77 All studies noted that regions of higher surface roughness values correlate with regions of  
78 higher crater density (the cratered terrain [e.g., *Trask and Guest*, 1975; *Spudis and Guest*,  
79 1988; *Whitten et al.*, 2014]) and regions of lower surface roughness values correlate with  
80 regions of lower crater density (the smooth plains [e.g., *Trask and Guest*, 1975; *Spudis*  
81 *and Guest*, 1988; *Denevi et al.*, 2013]). In addition, both *Fa et al.* [2016] and *Susorney*  
82 *et al.* [2017] saw noticeable increases in surface roughness values around individual large  
83 craters located in the smooth plains.

84 In the current study, we build upon previous investigations of the surface roughness of  
85 Mercury and focus on the surface roughness created by large impact craters. We limit  
86 this study to large craters (diameter  $> 20$  km) since previous studies have observed that  
87 the regional surface roughness of Mercury is dominated by such craters [*Kreslavsky et al.*,  
88 2014; *Fa et al.*, 2016; *Susorney et al.*, 2017]. In particular, we want to investigate the  
89 source of increased surface roughness around large craters (diameters  $> 80$  km) in the

90 smooth plains noted in *Fa et al.* [2016]; *Susorney et al.* [2017]. This study is composed  
91 of two parts: first, an in-depth analysis of how surface roughness is distributed in and  
92 around individual craters (section 2 and 3) and second, a numerical investigation (section  
93 4) where we utilize the measured surface roughness values (from the first part of the  
94 study). We use the results of both parts to understand how individual craters modify  
95 the surface roughness of Mercury, how collections of craters through time modify surface  
96 roughness, and how crater density is related to surface roughness (section 5).

## 2. Measurement of Surface Roughness

97 To understand how impact craters affect surface roughness on Mercury, we measured  
98 the surface roughness of 17 large craters (see Table S1 for list). We computed the sur-  
99 face roughness of large craters on Mercury using the Mercury Laser Altimeter (MLA)  
100 tracks [*Zuber et al.*, 2012]. Using the topography from an individual laser altimetry track  
101 to calculate surface roughness is more accurate than using derived gridded topographic  
102 products, which typically are generated by binning and smoothing topography to fill in  
103 the topography in regions where no altimetry data are present [see discussion in *Glaze*  
104 *et al.*, 2003; *Barnouin-Jha et al.*, 2005; *Robbins and Hynek*, 2013]. Because MLA tracks  
105 are concentrated in Mercury's northern hemisphere this investigation uses craters in the  
106 northern hemisphere.

107 We used root-mean-square (RMS) deviation as our measure of surface roughness; RMS  
108 deviation is the RMS change in detrended height over a given horizontal scale. We choose  
109 to use RMS deviation rather than other measures of surface roughness [e.g., *Kreslavsky*  
110 *et al.*, 2013] for several reasons. First, RMS deviation is commonly used in planetary radar  
111 and laser altimetry surface roughness studies [e.g., *Rosenburg et al.*, 2011; *Orosei*, 2003;



112 *Fa et al.*, 2016] and terrestrial surface roughness studies [e.g., *Mark and Aronson*, 1984].  
113 Second RMS deviation is related to the proposed self-affine behavior of natural surface s  
114 [e.g., *Turcotte*, 1997]. If RMS deviation is plotted against the baselines in a log-log plot  
115 and the resulting plot is linear in log-log space a Hurst exponent can be fit to the data.  
116 A single diagnostic Hurst exponent for a surface has been postulated to indicate that its  
117 topography is the result of a single geologic process without any characteristic scale [e.g.,  
118 *Shepard et al.*, 2001]. Additionally, previous studies exploring the relationship between  
119 surface roughness and crater densities used other measures of surface roughness rather  
120 than RMS deviation (median differential slope, [*Yokota et al.*, 2014] and topographic  
121 power spectra [*Rosenburg et al.*, 2015]). This permits us to explore the relationship of a  
122 different surface roughness parameter and crater density.

123 Larger regional maps of RMS deviation were presented in *Susorney et al.* [2017], and  
124 were used to understand the relative contribution of volcanism, tectonics, and impact  
125 cratering to regional surface roughness. In this section, we will briefly review RMS devia-  
126 tion and its relationship to the self-affine nature of topography and how we filtered MLA  
127 data before measuring RMS deviation. We then explain how surface roughness maps were  
128 produced and how radial plots of surface roughness around large craters were generated.

## 2.1. Measurements from MLA data

129 The surface roughness was measured at baselines of 0.5-250 km with the smallest base-  
130 line being constrained by the spacing between individual returns along an MLA track,  
131 which vary from 0.3-0.7 km. Individual MLA points were evaluated for each baseline  
132 investigated to check that the spacing between MLA points within five times the baseline  
133 on either side of the point was less than the baseline investigated [see *Susorney et al.*,

134 2017]. If the MLA point had appropriate spacing, adjacent MLA points within five times  
 135 the baseline were interpolated to generate a spacing equivalent to the baseline being mea-  
 136 sured. In *Susorney et al.* [2017] this methodology (see Fig. 3 in *Susorney et al.* [2017])  
 137 was compared to topography that was not interpolated and no statistical difference in  
 138 the resulting surface roughness values was found. Then, ten times the baseline of interest  
 139 was detrended to remove broad-scale slopes (five times on either side of the MLA point,  
 140 following recommendations in *Shepard et al.* [2001]). The difference in height one baseline  
 141 up and one down from the MLA point was then measured. The change in height  $[\Delta h(L)_i]$   
 142 was then used to calculate  $\nu(L)$  using Eqn. (1).

## 2.2. RMS Deviation

RMS deviation,  $\nu(L)$ , is the change in detrended topographic height,  $h$ , over a given horizontal baseline,  $L$ , and is defined by

$$\nu(L) = \left\{ \frac{1}{n} \sum_{i=1}^n [\Delta h(L)_i]^2 \right\}^{\frac{1}{2}}, \quad (1)$$

where  $\Delta h(L)_i$  is the change in height and  $i$  is the number of  $\Delta h$  used to calculate RMS deviation. RMS deviation is related to the Hurst exponent,  $H$ , which describes how the surface roughness changes with increasing baseline by

$$\nu(L) = \nu_o L^H, \quad (2)$$

143 where  $\nu_o$  is the RMS deviation at the unit scale. If the surface has self-affine-behavior a  
 144 straight line can be fit to the log of  $L$  versus the log of  $\nu(L)$  and the resulting exponent of  
 145 the fit to the line is  $H$  [*Turcotte*, 1997]. It has been postulated that when a single  $H$  exists  
 146 for a surface then a single geologic process without any characteristic scale might control  
 147 the observed topography [e.g., *Shepard et al.*, 2001]. When referring to the results of this

148 study surface roughness and RMS deviation are used interchangeably. RMS deviation  
149 was calculated from the data in two ways. For the maps, the  $\Delta h$  was gridded across the  
150 surface into grid sizes twice the baseline of interest, then RMS deviation was calculated  
151 for each grid point. For the radial plots, the  $\Delta h$  were sorted into radial 1 km bins around  
152 the crater and if more than 100  $\Delta h$  were found in each bin RMS deviation was calculated.  
153 We required at least 100  $\Delta h$  to be in each bin because RMS deviation is unstable below  
154 this threshold for Mercury [*Susorney et al.*, 2017].

### 2.3. Maps of Surface Roughness

155 To understand how the surface roughness is distributed in and around large craters  
156 on Mercury, we generated maps of surface roughness centered on large craters using the  
157 Generic Mapping Tools (GMT, <http://gmt.soest.hawaii.edu>, *Wessel et al.* [2013]). Maps  
158 were gridded at twice the baseline at which the surface roughness was computed to avoid  
159 smearing. This, for example, meant that a map at  $L = 1$  km would be gridded at 2 km. A  
160 continuous curvature spline fit was added to ease presentation of data [*Smith and Wessel*,  
161 1990]. Maps without spline fits were consulted to check that no artifacts were introduced  
162 by these fits. Maps were used for qualitative comparisons only since due to sparse MLA  
163 coverage the required 100  $\Delta h$  were not in each gridded bin.

### 2.4. Surface Roughness Radial Analysis

164 In addition to the maps of surface roughness, we also calculated radial profiles of surface  
165 roughness around the large craters. For each crater, we sorted all measurements of  $\Delta h$   
166 into their radial distance from the center of the crater. We then calculated the RMS

167 deviation for 1-km-wide bins (e.g. the RMS deviation of all  $\Delta h$  that were 0-1 and then  
168 1-2 km away from the center of the crater).

### 3. Surface Roughness Observations of Large Craters

169 In this section, we use the roughness data products described above to assess the surface  
170 roughness in and around large craters on Mercury and how the distribution of surface  
171 roughness changes with crater diameter. We first look at large craters with diameters  
172 ( $d$ ) greater than 50 km, then at large craters with  $d < 50$  km, and then at an unusual  
173 crater, Hokusai. Finally, we use the crater Abedin as a case study for studying the spatial  
174 relationship of specific crater attributes and the measured surface roughness for craters  
175 with diameters larger than 50 km. In Fig. 1 you can see the locations of craters studied  
176 on the surface of Mercury.

#### 3.1. Craters with diameters over 50 km, $d > 50$ km

177 The surface roughness maps of five relatively fresh craters at  $L = 1$  km (two of which  
178 are on the same map) are shown in Fig. 2, the first four of these craters have diameters  
179 larger than 50 km. All five of these craters lie in the smooth plains (region of lower crater  
180 density compared with the heavily cratered terrain) where the pre-existing topography  
181 is qualitatively smooth and is not an important contributor to the surface roughness  
182 measured at and around these craters [*Kreslavsky et al.*, 2014; *Fa et al.*, 2016; *Susorney*  
183 *et al.*, 2017]. This study will focus on the surface roughness of fresh craters where the  
184 surface roughness has been minimally affected by degradation. The five craters in Fig. 2  
185 are considered fresh and minimally degraded [*Susorney et al.*, 2016] and all the craters

186 measured in this study do not appear to have their surface roughness strongly affected by  
187 crater degradation.

188 The craters Abedin (Fig. 2(a-c)), Stieglitz (the larger crater in Fig. 2(d-f)), and Gaudi  
189 (the medium-sized crater in Fig. 2(d-f)) all show surface roughness distributions typical  
190 of craters with diameters over 50 km on Mercury. They have smaller surface roughness  
191 values in the crater floor, greater values near the central peak and rim, and a large region  
192 of high surface roughness values beyond the crater rim. For the 1 km baseline, the range in  
193 surface roughness values is from 0.001–0.25 km. This region of enhanced surface roughness  
194 exterior to the crater rim is not easily attributed to a single aspect of crater morphology  
195 and occurs over a region that includes both the continuous ejecta and the secondary crater  
196 fields.

197 Radial plots of the  $L = 1$  km surface roughness of Abedin, Gaudi, and Stieglitz are  
198 shown in Figure 3(a-c) and are also plotted against the radial MLA topography measured  
199 in the same 1-km radial bins. The radial plots show the same pattern as the maps, with  
200 increased surface roughness values around the central uplift (peak or ring) and the crater  
201 rim; the crater floors have decreased surface roughness.

202 The radial surface roughness plots of Abedin and Stieglitz show a decrease immediately  
203 exterior to the crater rim, but then an increase to form a qualitative local maximum  
204 [Fig. 3(a)]. We identified this qualitative local maximum in surface roughness through a  
205 visual inspection of the crater plots (see Figs. S1 and S2). Six of the 17 crater measured  
206 exhibit this qualitative local maximum and all of the craters that had the qualitative local  
207 maximum are larger than 100-km in diameter. In Fig. 3(f) we plot the diameter of the  
208 crater studied versus whether it had a qualitative local maximum outside of the crater

209 rim. When we produced radial plots of these same craters at  $L = 0.5$  km (Figs. S3-S5),  
210 we still observe a qualitative local maximum for those craters where it was previously  
211 identified (for the  $L = 1$  km), but also observed local maxima for different craters that  
212 are 80-100 km diameters indicating that the presence of a qualitative local maximum in  
213 the surface roughness exterior to the crater scales with crater diameter and the horizontal  
214 scale over which surface roughness is measured.

215 Plots of the radial profile of surface roughness for the crater Abedin at  $L = 0.5, 5, 20,$   
216 and 100 km are shown in Figure 4. The  $L = 0.5$  km radial plot shows the same general  
217 qualitative local maximum as  $L = 1$  km, but it disappears in the  $L = 5$  km and larger  
218 baseline radial plots. In the  $L = 20$  and 100 km radial plots, the surface roughness does  
219 not have high surface roughness values associated the central uplift and rim; instead, there  
220 is just a single increase in surface roughness associated with the crater cavity.

221 In the smooth plains only two craters with diameters over 50 km have overlapping  
222 ejecta/secondary fields, Gaudi and Stieglitz. In the map of Gaudi and Stieglitz [Fig.  
223 2(d-f)], the regions of increased roughness values surrounding the craters overlap, but  
224 the measured roughness values are not additive when the ejecta and secondary fields are  
225 superposed. In addition, the enhanced surface roughness exterior to the crater overprints  
226 the surface roughness from pre-existing smaller craters. The surface roughness did not  
227 co-add in any of the baselines investigated. This supports observations in images of the  
228 surface of Mercury, that show overlapping ejecta combining to produce a similar visual  
229 texture *Whitten et al.* [2014]. Additionally, the radial plots of Gaudi and Stieglitz (Fig.  
230 2(b) and (c) show similar surface roughness values to each other and are not higher than  
231 the surface roughness values of the crater Abedin (Fig. 2(a)). If the surface roughness was

232 co-adding we may expect the surface roughness of Gaudi and Stieglitz to be higher than  
233 other craters that are not adjacent to other fresh large craters. Also, a radial analysis of  
234 the surface roughness of Stieglitz broken into four quadrants (Fig. S6) around the crater  
235 show no differences in the surface roughness as would be expected in the northern two  
236 quadrants if the surface roughness was co-adding with the surface roughness of Gaudi.

### 3.2. Craters with diameters under 50 km

237 Craters with diameters under 50 km such as Egonu (Fig. 2(j-l),  $d = 25.0$  km) have  
238 surface roughness attributes similar to craters over 50 km in diameter within the crater  
239 cavity. Egonu has increased roughness values at its rim and central peak, and reduced  
240 values on the crater floor. However, Egonu does not possess a region of increased surface  
241 roughness exterior to the crater rim. The radial plot of Egonu [Fig. 3(e)] confirms this  
242 pattern: interior to the crater rim, the measured roughness is similar to craters over 50  
243 km in diameter, but no qualitative local maximum is found exterior to the crater rim,  
244 consistent with the diameter and baseline dependency noted before. Three additional  
245 craters (Grotell, Riveria, and Martial, see Figs. S1 and S2) with diameters near or under  
246 50 km show the same pattern in surface roughness as Egonu.

### 3.3. Hokusai, an unusual large crater on Mercury

247 Hokusai (Fig. 2(g-i) and Fig. 3(d)) is a notable exception to the pattern outlined above  
248 for craters with diameters greater than 50 km in the smooth plains. The map of the  
249 surface roughness of Hokusai has a smaller region of enhanced surface roughness values  
250 compared to other craters over 50 km in diameter (e.g., Abedin). Previous studies of  
251 Hokusai have noted extensive melt and unusual ejecta [rampart like structures, *Xiao and*

252 *Komatsu, 2013; Barnouin et al., 2015; Xiao et al., 2016*]. Arecibo radar data noted a  
253 region of elevated roughness values around Hokusai [*Harmon et al., 2007*] likely due to  
254 Hokusai having extensive melt, which is rough in radar-scale (S-band) surface roughness  
255 [*Neish et al., 2013*] due to the centimeter-scale structure and smooth at  $L = 1$  km surface  
256 roughness since melt will infill ‘rougher’ topography. Additionally, *Xiao et al.* [2014]  
257 reported a lower density of secondary craters surrounding Hokusai. Impact melt exterior  
258 to the crater rim would explain the lower  $L = 1$  km surface roughness values since melt  
259 would infill the regions of higher surface roughness values observed in other craters over  
260 50 km in diameter. It is also possible that extensive melt in the ejecta reduced the  
261 strength of blocks in the ejecta and thus the number of secondary craters around Hokusai  
262 [e.g., *Schultz and Singer, 1980*]. The lower density of secondary craters could result in  
263 lower surface roughness values exterior to the crater rim. Hokusai is also likely one of  
264 the youngest craters on the planet due to its degradation state [*Susorney et al., 2016*],  
265 but there are also very fresh craters on the surface that do not display the same amount  
266 of melt as Hokusai. Additionally, the MLA coverage around Hokusai is not as dense as  
267 the coverage around Abedin, but in the radial surface roughness plots had sufficient  $\Delta h$   
268 present to calculate RMS deviation.

### 3.4. Abedin

269 To investigate the origin of the qualitative local maximum in the  $L = 1$  km surface  
270 roughness maps and profiles, we investigate in detail the relatively fresh crater Abedin.  
271 In particular, we focus on whether secondaries or ejecta is the source of elevated surface  
272 roughness exterior to the crater,

#### 3.4.1. Geologic map of Abedin



274 The geology of Abedin was mapped (Fig. 5) using a 250 m/pixel Mercury Dual Imaging  
275 System mosaic. The mapping was performed on a sphere in the Small Body Mapping Tool  
276 (SBMT) [e.g., *Kahn et al.*, 2011]. We focused on identifying the radial limits of the ejecta,  
277 crater floor, central peak, and rim. In Fig. 6 we marked the radial extent of the crater  
278 floor, ejecta, and secondary fields on a radial surface roughness plot. The qualitative local  
279 maximum straddles the continuous ejecta and secondary fields.

### 280 3.4.2. Density of secondary craters around Abedin

281 To investigate whether secondary craters are correlated with the qualitative local maxi-  
282 mum exterior to the crater rim, we compared secondary crater density to surface roughness  
283 by mapping all secondary craters (we assumed all small craters, diameters under 10 km,  
284 that were outside of Abedin’s rim were secondaries for this part of the study) over 1 km  
285 in diameter within six crater radii of the center of Abedin. Over 7000 secondary craters  
286 >1 km in diameter were identified in the Small Body Mapping Tool [*Kahn et al.*, 2011]  
287 using the same 250 m/pixel Mercury Dual Imaging System mosaic. In Figure 7 the radial  
288 density (in 1 km bins) of secondary craters (1-10 km in diameter) is plotted with the  $L =$   
289 1 km surface roughness of Abedin against the distance from the center of Abedin. We cal-  
290 culated the density of secondary craters in 1 km radial bins and took the total number of  
291 craters in the annulus and divided by the area of the annulus. The maximum in secondary  
292 crater density is farther from the crater center than the local surface roughness maximum.  
293 This observation implies that secondary craters are not the only source of the qualitative  
294 local maximum. A mixture of the continuous ejecta and secondary craters is likely the  
295 source of this qualitative local maximum, given that it is straddling the transition between  
296 these two regions.

## 4. Numerical Investigations

297 We used a numerical investigation to understand how the formation of multiple impact  
298 craters influences the regional surface roughness of Mercury. These simulations did not try  
299 to re-create the actual topography of a cratered surface [e.g., *Gaskell*, 1993; *Richardson*,  
300 2009; *Yang et al.*, 2013; *Rosenburg et al.*, 2015], which must make assumptions of the  
301 topography created by craters. Instead, we used the measured surface roughness values in  
302 and around large craters on Mercury (the results from section 3) to test whether we can  
303 re-create aspects of the regional surface roughness observed on Mercury in the smooth  
304 plains and cratered terrains using fresh large craters alone.

### 4.1. Investigation set-up and assumptions

305 In this investigation, we used the measured radial distribution of surface roughness (at  
306 all baselines measured of 0.5–250 km) out to four crater radii from the center of five  
307 large craters ranging in diameter from 25–100 km. Details about the five craters selected  
308 are in Table 1. The range of crater diameters were chosen to match the five bin sizes  
309 used in crater counts by *Ostrach et al.* [2015], who investigated the crater size-frequency  
310 distribution on the smooth plains and the cratered terrains of Mercury. An artificial  
311 1000-km-by-1000-km surface was generated with an initial surface roughness of 0.0 km.  
312 Changing this initial value to match background (non-large cratered) surface roughness,  
313 for example, was found to have no influence on the final outcome of the roughness com-  
314 puted for the artificial surface (Fig. S7). The  $\Delta h$  from the radial distribution of surface  
315 roughness of the five craters were then added to random locations on the surface and  
316 RMS deviation was calculated from this. The location of each crater was based on the

317 size-frequency measured by *Ostrach et al.* [2015] for either the smooth plains or cratered  
318 terrain [see Fig. 8(a) and (d)].

319 We performed more computationally expensive simulations using a 2000-km-by-2000-  
320 km surface measured in the same manner above and the 2000-km-by-2000-km surface  
321 where we only measured the center 1000-km-by-1000-km surface to check for any bound-  
322 ary effects. The results of both of these simulations are found in the supplementary  
323 information (Figure S8 and S9) and the Hurst exponent and shape of the devioqram mea-  
324 sured from these two simulations are not different from the simulations run in the original  
325 1000-km-by-1000-km configuration.

326 When a new crater was added to the surface, its roughness overprinted any pre-existing  
327 surface roughness. This assumption prevented us from introducing additional complexity  
328 to our numerical simulation. Additionally, observations of Gaudi and Stieglitz showed that  
329 overlapping regions of elevated surface roughness did not co-add and that there surface  
330 roughness overprinted surface roughness due to an older crater in the region.

331 Craters were added to the surface until the simulated size-frequency distribution on  
332 the surface matched either the smooth plains or cratered terrain as measured by *Ostrach*  
333 *et al.* [2015]. The surface roughness of the complete 1000-km-by-1000-km surface was  
334 recalculated after each crater was added (Fig. 8(c) and (f)). We also calculated the Hurst  
335 exponent from baselines of 0.5-1.5 km, the same baselines found to have self-affine-like  
336 behavior in *Susorney et al.* [2017].

## 4.2. Results of the numerical investigation

337 Figs. 9 and 8 show the simulated surface roughness, crater-size-frequency, and de-  
338 viogram (RMS deviation versus baseline) of simulated regions where the final crater den-

339 sities match the smooth plains and cratered terrain, respectively. Fig. 10 compares the  
340 final devioqram for 30 runs for the simulated smooth plains and cratered terrain to the  
341 measured surface roughness of the two regions on Mercury obtained in *Susorney et al.*  
342 [2017].

343 At baselines of 0.5–1.5 km, the simulated devioqrams are approximately linear resulting  
344 in Hurst exponents of  $0.98 \pm 0.01$  and  $0.99 \pm 0.00$  for the smooth plains and cratered  
345 terrains, respectively. We choose the baselines of 0.5–1.5 to match the baselines a Hurst  
346 exponent was fit to in [*Susorney et al.*, 2017] since we compared the results of the simula-  
347 tion to the results of that paper. The values of the Hurst exponent are the mean of thirty  
348 separate simulations and the uncertainties are one standard deviation of the thirty runs.  
349 These Hurst exponents are larger than the measured  $H$  of the cratered terrain (0.95) and  
350 smooth plains (0.88) for the same baselines [*Susorney et al.*, 2017]. *Fa et al.* [2016] mea-  
351 sured different Hurst exponents for the smooth plains (0.60) and cratered terrain (0.80)  
352 of Mercury, but these were measured over a broader range of baselines ( $L = 0.4$ – $4.2$  km).  
353 There could be many reasons for the larger Hurst exponent in our models compared to  
354 observations, a larger Hurst exponent means that topography is larger for longer baseline  
355 compared to a small Hurst exponent. This larger increase in topography could be due to  
356 the lack of degradation in our models or the lack of small craters.

357 The shape of the devioqram at  $L < 40$  km is reproduced in the numerical investigation.  
358 However, the simulated and measured devioqrams do not overlap each other, with the sim-  
359 ulated devioqram having a lower overall surface roughness than the measured devioqram  
360 at all baselines. A second measured devioqram of the smooth plains from measured sur-  
361 face roughness values is also plotted in Fig. 10 (Smooth Plains 2). This second devioqram

362 of the smooth plains was measured away from the smooth plains unit boundary, where  
363 boundary effects from the cratered terrain can influence the surface roughness (see *Su-*  
364 *sorney et al.* [2017]). In this second devioqram, the measured devioqram and simulated  
365 devioqram are closer in agreement, with a bend in the surface roughness around  $L =$   
366 30 km being reproduced although the measured surface roughness of Smooth Plains 2  
367 is larger than the simulated surface roughness of the smooth plains. The lower surface  
368 roughness values in our simulation compared to measured surface roughness on Mercury  
369 is likely due to a combination of the lack of simple craters, tectonics, and large basins [*Fa-*  
370 *et al.*, 2016; *Susorney et al.*, 2017] and the complete overprinting of the surface rough-  
371 ness of pre-existing craters in our simulations. In particular, the lack of degradation and  
372 complete overprinting of pre-exsisting surface roughness is likely not an accurate repre-  
373 sentation of the evolution of highly cratered surfaces however, it is difficult to tease apart  
374 how the surface roughness of many impact craters interact in heavily cratered surfaces.  
375 The role of smaller diameter craters may be important in driving the evolution of surface  
376 roughness as small diameter craters are an important aspect in crater equilibrium on a  
377 surface *Xiao and Werner* [2015].

## 5. Discussion

378 In this section, we use both observations of the surface and numerical simulations to  
379 understand how large craters produce and modify surface roughness on Mercury. We also  
380 assess any relationship between measured surface roughness produced by large craters and  
381 crater density.

## 5.1. Individual large craters

382 Our results indicate that the distribution of surface roughness around large craters on  
383 Mercury at smaller baselines ( $L < 10$  km) is well correlated with the morphology of the  
384 crater. The largest regional contributor to surface roughness is the area exterior to the  
385 crater rim. A few large ( $d > 80$  km) large craters can completely dominate the local surface  
386 roughness of terrain with a few impact craters (e.g., the smooth plains on Mercury). This  
387 finding supports observations by *Fa et al.* [2016]; *Susorney et al.* [2017] that individual  
388 large craters appear to dominate the surface roughness at smaller baselines. Simulations  
389 measuring the surface roughness by *Yokota et al.* [2014] produced by simulated craters  
390 (modeled as modified cones) didn't reproduce the local maxima in roughness at baselines  
391 of 6–9 km that was associated with impact craters. The authors hypothesized it was due  
392 to the lack of realistic ejecta and secondary craters in their simulations. Our observation  
393 of the importance of ejecta and secondary fields for surface roughness at baselines under  
394 10 km support the authors' hypothesis.

## 5.2. Interaction of multiple impact craters

395 Our observations of the surface roughness of the craters Gaudi and Stieglitz with their  
396 overlapping ejecta and secondary fields show that the surface roughness of the exterior  
397 of craters does not co-add, but simply overprints. Observations of the cratered terrain  
398 on Mercury noted that the qualitative rough texture of the cratered terrain is created by  
399 overlapping ejecta blankets [*Whitten et al.*, 2014]. This qualitative observation is similar  
400 to our observation of the importance of the region exterior to craters (in particular when  
401 these regions overlap) to increasing the surface roughness of an entire region at small  
402 baselines ( $L < 10$  km).

403 The numerical investigation yielded  $H$  values for the simulated smooth plains and  
404 cratered terrain of  $0.998 \pm 0.01$  and  $0.99 \pm 0.00$  are similar to the measured  $H$  of the  
405 cratered terrain ( $0.95 \pm 0.01$ ) at the same baselines and the lunar highlands where  $H$   
406  $= 0.95$  for  $L = 0.017$ - $2.7$ . The similarity among all these Hurst exponents may support  
407 the hypothesis that a Hurst exponent is indicative of a single geologic process without a  
408 diagnostic scale controlling surface roughness at these scales [e.g., *Shepard et al.*, 2001;  
409 *Rosenburg et al.*, 2011], in this case, impact cratering.

### 5.3. Surface roughness and crater density

410 Previous studies have proposed that surface roughness can be used to estimate surface  
411 age since regions with higher surface roughness values usually have higher crater densities  
412 [e.g., *Yokota et al.*, 2014]. Here, we can use our results to investigate how surface roughness  
413 changes with increasing crater density. Fig. 11 shows our surface roughness values for  
414 the entire simulated region after increasing numbers of large craters are emplaced on a  
415 region for the cratered terrain simulation in Section 5 (for  $L = 0.5, 1, 5, 10, 40$  km).  
416 The gray region represents the one standard deviation of 30 runs. The plot indicates  
417 that after 15 craters are emplaced, the surface roughness for  $L = 0.5$  and 1 km does  
418 not increase but remains constant. When the surface roughness does not change with  
419 increasing number of craters we believe the region is in "steady-state surface roughness".  
420 The surface roughness at 5 and 10 km baselines reaches a steady-state after  $\sim 30$  craters  
421 are added. The  $L = 40$  km surface roughness reaches a steady-state after  $\sim 80$  craters are  
422 added, but the uncertainty is large. Surfaces dominated by large craters reach a surface  
423 roughness steady-state before the surface is completely covered in craters at the baselines  
424 investigated.

425 At  $L < 10$  km, the surface roughness measured is dominated by the region exterior to  
426 the crater rim and covers a large surface area. It should not, therefore, be surprising that  
427 at these baselines the roughness reaches a steady-state after only a few craters form. This  
428 result shows that it is not possible to relate the surface roughness at smaller baselines to  
429 crater density/surface age on Mercury for terrains similar to the cratered terrain. At  $L >$   
430 10 km, the surface roughness generated by a single crater is dominated by that crater's  
431 cavity. Thus, for these longer baselines, the time required to reach surface roughness  
432 steady-state is longer. This is consistent with the results of *Yokota et al.* [2014], who found,  
433 with their idealized crater shapes and cavities as the main source of surface roughness in  
434 the simulations, that a correlation existed between surface roughness for  $L$  between 20-  
435 30 km and crater density  $N(>20\text{km})$ . In our investigation, we find that for baselines  
436 of 20–40 km it is difficult to identify a simple relationship between crater density and  
437 surface roughness alone since there is some variation in this relationship, as seen in Fig.  
438 11 where variation between simulations for these larger baselines is quite large. While  
439 we can not rule out using the surface roughness at larger baselines as a proxy for crater  
440 density/surface age, the variation in the relationship would always be a larger source of  
441 uncertainty in any result.

## 6. Conclusions

442 For many planetary bodies, impact craters are the dominant source of surface roughness.  
443 In this paper, we have investigated how large craters influence the surface roughness of  
444 Mercury. The main results of our study are:

- 445 1. For baselines  $L < 10$  km, large craters on Mercury have larger surface roughness  
446 values at the crater rim and central peak and lower values on the crater floor. The region



447 exterior to the crater rim is the largest areal source of surface roughness for these baselines.  
448 Exterior to fresh large craters (diameters  $> 80$  km) there is a qualitative local maximum  
449 in surface roughness that occurs in a region that includes both continuous ejecta and  
450 secondary fields.

451 2. When multiple large impact craters occur near each other the resulting region of  
452 elevated surface roughness exterior to the crater rims do not co-add, but instead merge  
453 and results in a region reaching surface roughness steady-state rapidly as these regions of  
454 high surface roughness merge.

455 3. For  $L > 10$  km, the surface roughness is primarily due to the crater's cavity (the  
456 decrease in elevation from the rim to the crater floor).

457 4. The large crater Hokusai has a smaller region of increased surface roughness values  
458 exterior to the crater rim as compared to similarly size fresh large craters. This reduction  
459 in surface roughness values is likely due to the large amount of impact melt in and around  
460 Hokusai and fewer number of secondary craters.

461 5. A numerical investigation into whether large craters alone can produce the surface  
462 roughness measured on Mercury found that the majority of the surface roughness of  
463 the smooth plains and cratered terrain can be attributed to large craters, but not all.  
464 The Hurst exponent from the numerical investigation for both the smooth plains and  
465 cratered terrain is similar to the Hurst exponent of Mercury's cratered terrain and the  
466 lunar highlands.

467 6. The relationship between surface roughness and crater density varies based on base-  
468 line investigated. At  $L < 10$  km, the region exterior to the crater dominates surface  
469 roughness and results in a surface reaching surface roughness steady-state after only a

470 few craters have been added to the surface. At  $L > 10$  km surface roughness appears to  
471 be linked with the crater cavity itself and could be a better proxy for age, although, there  
472 is some variation between identical numerical simulations.

### 473 **Acknowledgments.**

474 We would like to thank Drs. Hauck and Fa for editorial handling and Drs. Kreslavsky,  
475 Cao, and an anonymous reviewer for their comments that improved the paper. Support  
476 was provided by the Johns Hopkins University Applied Physics Laboratory Graduate  
477 Student Fellowship Program for H.C.M.S., and the Johns Hopkins University Applied  
478 Physics Laboratory Hafstad Fellowship program for O.S.B. We would like to acknowl-  
479 edge the Small Body Mapping Tool developed by the Johns Hopkins University Applied  
480 Physics Laboratory for geologic mapping in this study. Finally, we thank the scientists  
481 and engineers of the MESSENGER mission for the MLA dataset.

482 Data used in the creation of this paper will be released on Zenodo upon publication.

### References

- 483 Barnouin, O. S., C. M. Ernst, and H. C. M. Susorney (2015), The Remarkable Hokusai  
484 Crater, Mercury, *46th Lunar and Planetary Science Conference*, 46, 2672.
- 485 Barnouin-Jha, O. S., S. Baloga, and L. Glaze (2005), Comparing landslides to fluidized  
486 crater ejecta on Mars, *Journal of Geophysical Research*, 110(E), 4010.
- 487 Denevi, B. W., C. M. Ernst, H. M. Meyer, M. S. Robinson, S. L. Murchie, J. L. Whitten,  
488 J. W. Head, T. R. Watters, S. C. Solomon, L. R. Ostrach, C. R. Chapman, P. K. Byrne,  
489 C. Klimczak, and P. N. Peplowski (2013), The distribution and origin of smooth plains  
490 on Mercury, *Journal of Geophysical Research: Planets*, 118(5), 891–907.

- 491 Fa, W., Y. Cai, Z. Xiao, and W. Tian (2016), Topographic roughness of the northern high  
492 latitudes of Mercury from MESSENGER Laser Altimeter data, *Geophysical Research*  
493 *Letters*, p. doi:10.1002/2016GL068120.
- 494 Gaskell, R. W. (1993), Martian Surface Simulations, *Journal of Geophysical Research*,  
495 *98*(E6), 11,099–11,103.
- 496 Glaze, L. S., S. M. Baloga, and E. R. Stofan (2003), A methodology for constraining lava  
497 flow rheologies with MOLA, *Icarus*, *165*(1), 26–33.
- 498 Group, C. A. T. W. (1979), Standard techniques for presentation and analysis of crater  
499 size-frequency data, *Icarus*, *37*, 467–474.
- 500 Harmon, J. K., M. A. Slade, B. J. Butler, J. W. I. Head, M. S. Rice, and D. B. Campbell  
501 (2007), Mercury: Radar images of the equatorial and midlatitude zones, *Icarus*, *187*(2),  
502 374–405.
- 503 Kahn, E. G., O. S. Barnouin, D. L. Buczkowski, C. M. Ernst, N. Izenberg, S. Murchie,  
504 and L. M. Prockter (2011), A Tool for the Visualization of Small Body Data, *42nd*  
505 *Lunar and Planetary Science Conference*, *42*, 1618–.
- 506 Kreslavsky, M. A., and J. W. Head (2000), Kilometer-scale roughness of Mars: Results  
507 from MOLA data analysis, *Journal of Geophysical Research: Planets (1991–2012)*,  
508 *105*(E11), 26,695–26,711.
- 509 Kreslavsky, M. A., and J. W. Head (2016), The steepest slopes on the Moon from Lu-  
510 nar Orbiter Laser Altimeter (LOLA) Data: Spatial Distribution and Correlation with  
511 Geologic Features, *Icarus*, *273*, 329–336.
- 512 Kreslavsky, M. A., J. W. Head, and J. K. Harmon (2008), Large-Scale Topographic  
513 Roughness of Terrestrial Planets: A Comparison, *39th Lunar and Planetary Science*

514 *Conference*, 39, 1472.

515 Kreslavsky, M. A., J. W. Head, G. A. Neumann, M. A. Rosenburg, O. Aharonson, D. E.  
516 Smith, and M. T. Zuber (2013), Lunar topographic roughness maps from Lunar Orbiter  
517 Laser Altimeter (LOLA) data: Scale dependence and correlation with geologic features  
518 and units, *Icarus*, 226(1), 52–66.

519 Kreslavsky, M. A., J. W. Head, and G. A. Neumann (2014), Kilometer-scale topographic  
520 roughness of Mercury: Correlation with geologic features and units, *Geophysical Re-*  
521 *search Letters*, 41, 1–7.

522 Mark, D. M., and P. B. Aronson (1984), Scale-dependent fractal dimensions of topographic  
523 surfaces: An empirical investigation, with applications in geomorphology and computer  
524 mapping, *Mathematical geology*, 16(7), 671–683.

525 Neish, C. D., D. T. Blewett, J. K. Harmon, E. I. Coman, J. T. S. Cahill, and C. M.  
526 Ernst (2013), A comparison of rayed craters on the Moon and Mercury, *Journal of*  
527 *Geophysical Research: Planets*, 118(10), 2247–2261.

528 Orosei, R. (2003), Self-affine behavior of Martian topography at kilometer scale from Mars  
529 Orbiter Laser Altimeter data, *Journal of Geophysical Research*, 108(E4), 8023.

530 Ostrach, L. R., M. S. Robinson, J. L. Whitten, C. I. Fassett, R. G. Strom, J. W. Head,  
531 and S. C. Solomon (2015), Extent, age, and resurfacing history of the northern smooth  
532 plains on Mercury from MESSENGER observations, *Icarus*, 250, 602–622.

533 Pommerol, A., S. Chakraborty, and N. Thomas (2012), Comparative study of the surface  
534 roughness of the Moon, Mars and Mercury, *Planetary and Space Science*, 73(1), 287–  
535 293.

- 536 Richardson, J. E. (2009), Cratering saturation and equilibrium: A new model looks at an  
537 old problem, *Icarus*, *204*(2), 697–715.
- 538 Robbins, S. J., and B. M. Hynek (2013), Utility of laser altimeter and stereoscopic terrain  
539 models: Application to Martian craters, *Planetary and Space Science*, *86*, 57–65.
- 540 Rosenburg, M. A., O. Aharonson, J. W. Head, M. A. Kreslavsky, E. Mazarico, G. A. Neu-  
541 mann, D. E. Smith, M. H. Torrence, and M. T. Zuber (2011), Global surface slopes and  
542 roughness of the Moon from the Lunar Orbiter Laser Altimeter, *Journal of Geophysical*  
543 *Research*, *116*(E2), E02,001.
- 544 Rosenburg, M. A., O. Aharonson, and R. Sari (2015), Topographic power spectra of  
545 cratered terrains: Theory and application to the Moon, *Journal of Geophysical Re-*  
546 *search: Planets*, *120*(2), 177–194.
- 547 Schultz, P. H., and J. Singer (1980), A comparison of secondary craters on the Moon,  
548 Mercury, and Mars, *Lunar and Planetary Science Conference*.
- 549 Shepard, M. K., B. A. Campbell, M. H. Bulmer, T. G. Farr, L. R. Gaddis, and J. J. Plaut  
550 (2001), The roughness of natural terrain: A planetary and remote sensing perspective,  
551 *Journal of Geophysical Research*, *106*(E), 32,777–32,796.
- 552 Smith, W. H., and P. Wessel (1990), Gridding with Continuous Curvature Splines in  
553 Tension, *Geophysics*, *55*(3), 293–305.
- 554 Spudis, P. D., and J. E. Guest (1988), Stratigraphy and geologic history of Mercury, *IN:*  
555 *Mercury (A89-43751 19-91)*. Tucson, pp. 118–164.
- 556 Susorney, H., O. Barnouin, C. Ernst, and P. Byrne (2017), Surface Roughness of Mercury  
557 from MESSENGER, *Journal of Geophysical Research - Planets*, *in-press*, NA.

- 558 Susorney, H. C. M., O. S. Barnouin, C. M. Ernst, and C. L. Johnson (2016), Morphometry  
559 of impact craters on Mercury from MESSENGER altimetry and imaging, *Icarus*, *271*,  
560 180–193.
- 561 Trask, N. J., and J. E. Guest (1975), Preliminary geologic terrain map of Mercury, *Journal*  
562 *of Geophysical Research: Planets*, *80*(17), 2461–2477.
- 563 Turcotte, D. L. (1997), *Fractals and Chaos in Geology and Geophysics*, Cambridge Uni-  
564 versity, Cornell University, New York.
- 565 Wessel, P., W. H. F. Smith, R. Scharroo, J. Luis, and F. Wobbe (2013), Generic Mapping  
566 Tools: Improved Version Released, *Eos*, *94*(4), 409–410.
- 567 Whitten, J. L., J. W. Head, B. W. Denevi, and S. C. Solomon (2014), Intercrater plains on  
568 Mercury: Insights into unit definition, characterization, and origin from MESSENGER  
569 datasets, *Icarus*, *241*(C), 97–113.
- 570 Xiao, Z., and G. Komatsu (2013), Planetary and Space Science, *Planetary and Space*  
571 *Science*, *82-83*(C), 62–78.
- 572 Xiao, Z., and S. C. Werner (2015), Size-frequency distribution of crater populations in  
573 equilibrium on the Moon, *Journal of Geophysical Research: Planets*, *120*(12), 2277–  
574 2292.
- 575 Xiao, Z., R. G. Strom, C. R. Chapman, J. W. Head, C. Klimczak, L. R. Ostrach, J. Hel-  
576 bert, and P. D’Incecco (2014), Comparisons of fresh complex impact craters on Mer-  
577 cury and the Moon: Implications for controlling factors in impact excavation processes,  
578 *Icarus*, *228*, 260–275.
- 579 Xiao, Z., N. C. Prieur, and S. C. Werner (2016), The self-secondary crater population of  
580 the Hokusai crater on Mercury, *Geophysical Research Letters*, *43*(14), 7424–7432.

- 581 Yang, D., M. T. Zuber, J. W. Head, and S. C. Solomon (2013), Distribution of Topographic  
582 Slope and Roughness in Mercury’s Northern Hemisphere, *44th Lunar and Planetary*  
583 *Science Conference*, *44*, 2347.
- 584 Yokota, Y., K. Gwinner, J. Oberst, J. Haruyama, T. Matsunaga, T. Morota, H. Noda,  
585 H. Araki, M. Ohtake, S. Yamamoto, P. Gläser, Y. Ishihara, C. Honda, N. Hirata,  
586 and H. Demura (2014), Variation of the lunar highland surface roughness at baseline  
587 0.15-100 km and the relationship to relative age, *Geophysical Research Letters*, *41*(5),  
588 1444–1451.
- 589 Zuber, M. T., D. E. Smith, R. J. Phillips, S. C. Solomon, G. A. Neumann, S. A. Hauck II,  
590 S. J. Peale, O. S. Barnouin, J. W. Head, C. L. Johnson, F. G. Lemoine, E. Mazarico,  
591 X. Sun, M. H. Torrence, A. M. Freed, C. Klimczak, J.-L. Margot, J. Oberst, M. E. Perry,  
592 R. L. McNutt Jr, J. A. Balcerski, N. Michel, M. J. Talpe, and D. Yang (2012), Topog-  
593 raphy of the Northern Hemisphere of Mercury from MESSENGER Laser Altimetry,  
594 *Science*, *336*(6078), 217–220.

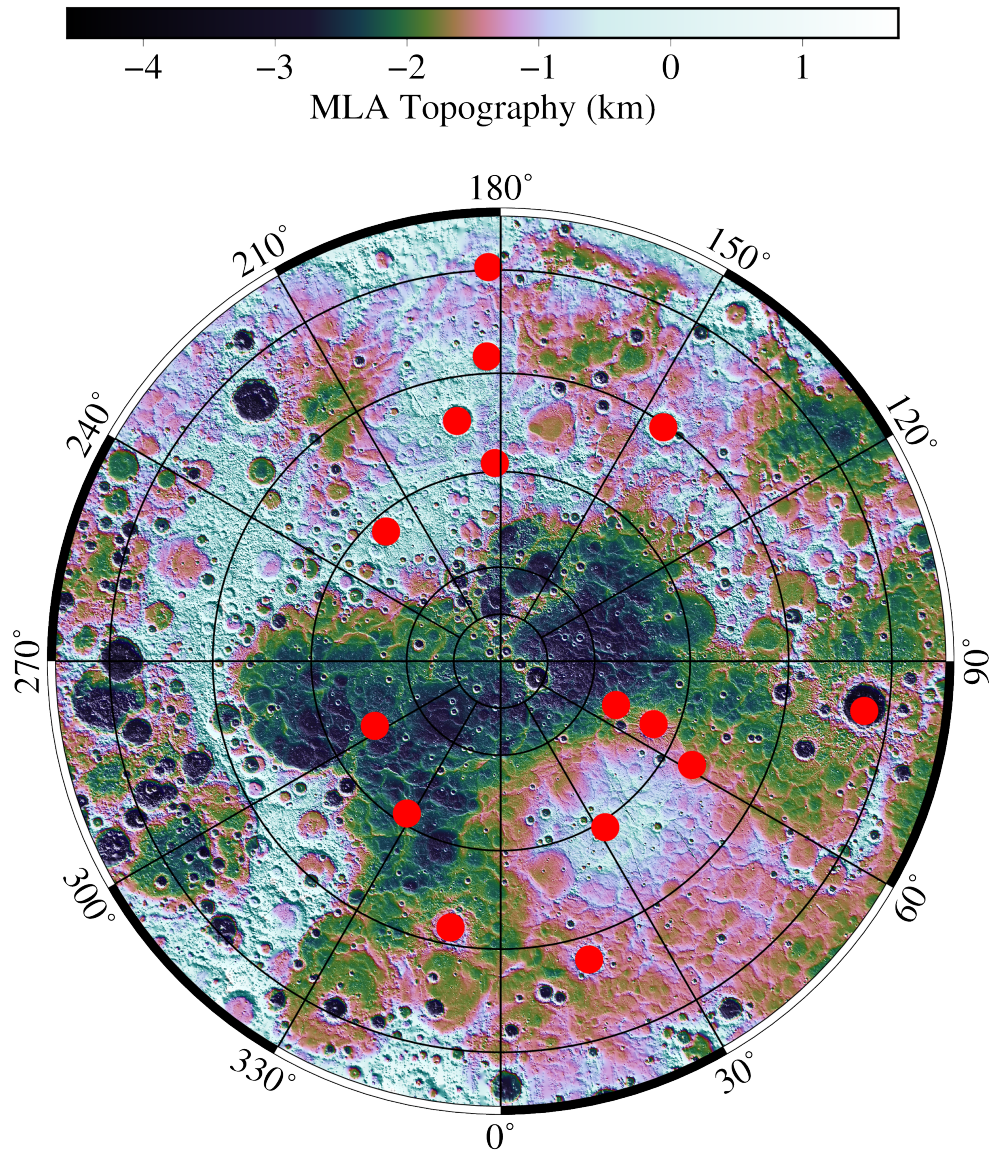


**Figure 1.** MLA topography map in a polar stereographic projection starting at  $45^\circ$  N with 16 of the 17 craters used in this study plotted as red dots in their respected location on the surface of Mercury. The crater Ahmad Baba is not plotted since its latitude is below  $45^\circ$  N.



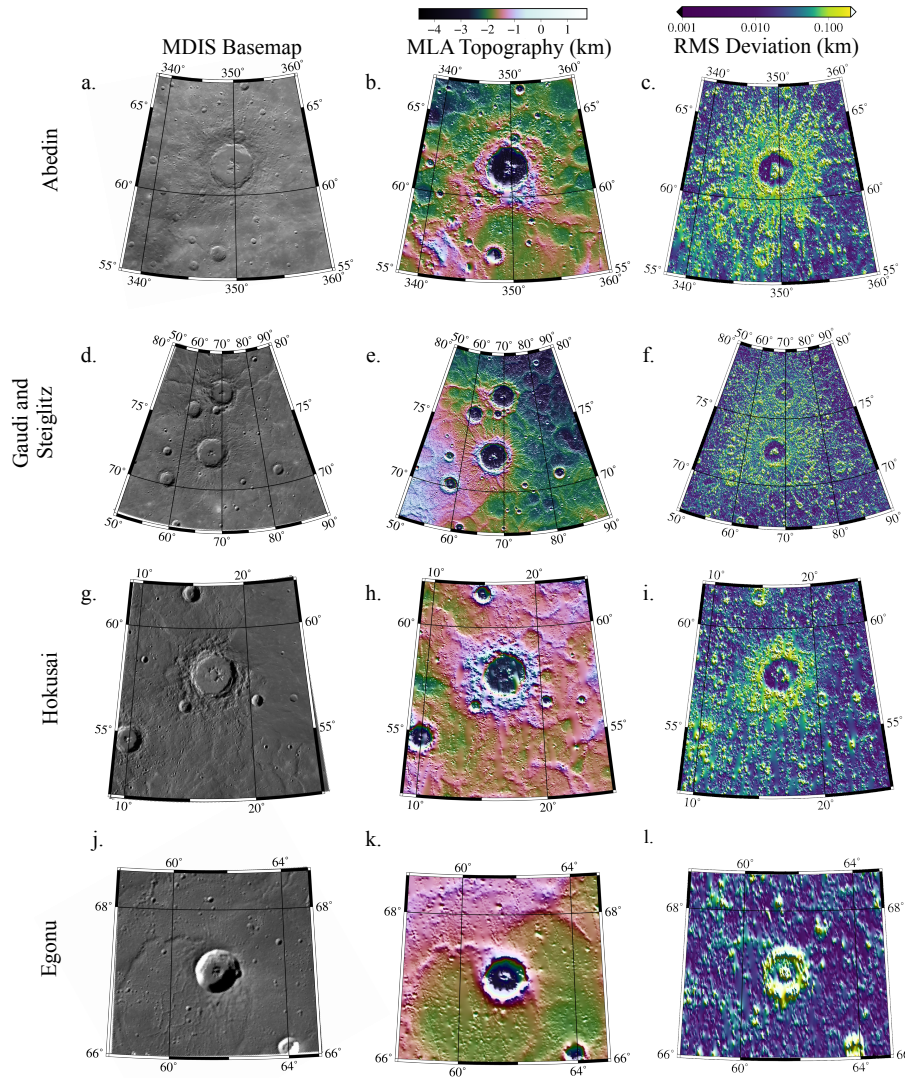


**Figure 2.** MDIS (Mercury Dual Imaging System) images (250 m/pixel basemap), MLA topography, and the  $L = 1$  km surface roughness for 5 impact craters on Mercury. (d)-(f) combine the images for Steiglitz and Gaudi. The craters Abedin ( $d = 122$  km), Gaudi ( $d = 81$  km), and Steiglitz ( $d = 100$  km) all show aerially broad regions of increased surface roughness beyond their rims. Hokusai ( $d = 97.3$  km), similar in size to Abedin, does not have as large of a region of high surface roughness as Abedin. The crater Egonu ( $d = 25$  km) does not show the same increased region of surface roughness surrounding the crater despite ejecta and secondary craters being visible in the MDIS image. Smaller craters might not produce sufficient fresh ejecta volume (or fragment size), nor fast enough secondary cratering to alter surface roughness significantly at the baselines investigated. Figure (l) appear more 'blurry' than (c) and (f) to

D R A F T

March 19, 2018, 8:52am

D R A F T

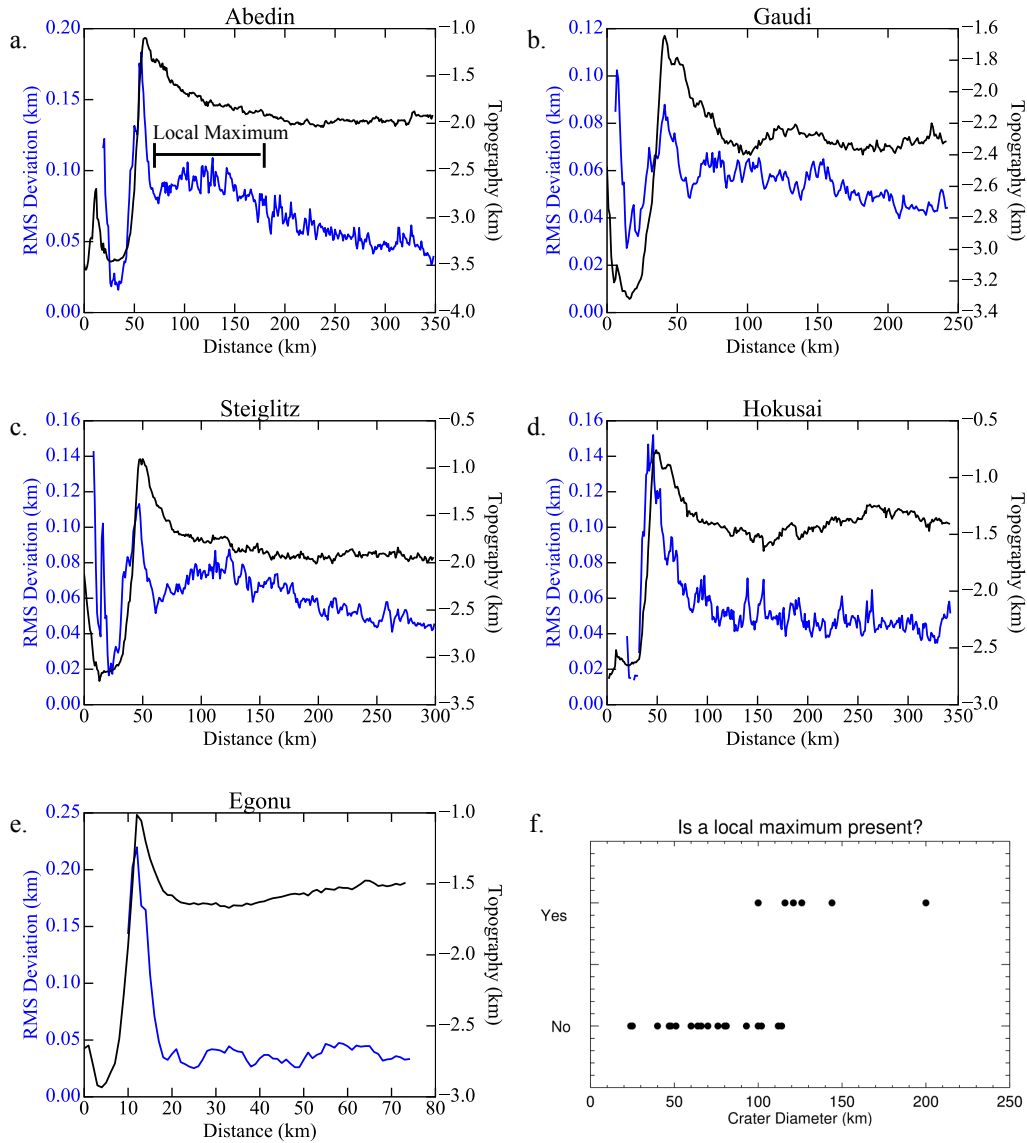


**Figure 3.** (a)-(e) RMS deviation for  $L = 1$  km (blue) and MLA topography (black) as a function of radial distance from the crater center for large craters mapped in Figure 1. Note the qualitative local maximum present around Abedin and Stieglitz, the diameters of craters with and without the qualitative local maximum is plotted in (f). The Trask freshness criteria classification [1-5 with 5 the freshest *Trask and Guest, 1975*] for the craters above are Abedin = 4, Gaudi = 3, Stieglitz = 4, Hokusai = 5, and Egonu = 4.

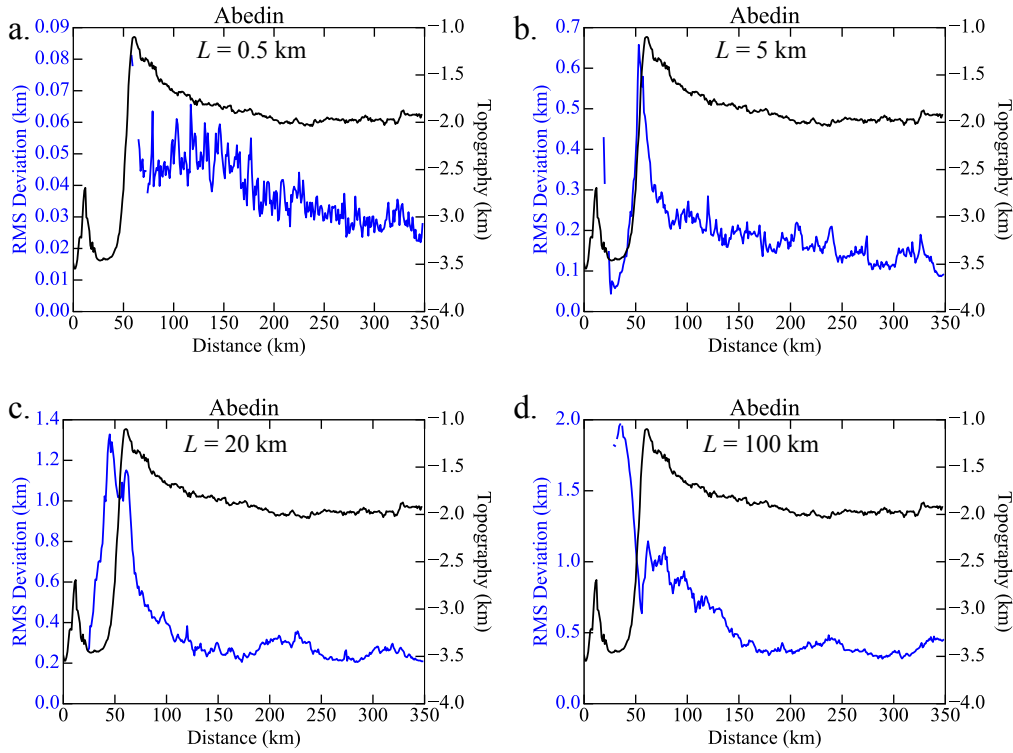


**Figure 4.** (a)-(d) RMS deviation and MLA topography in radial bins from the center of the crater Abedin for  $L = 0.5, 5, 20, 100$  km. The qualitative local maximum is only present at  $L = 0.5$  km and 1 km (previous figure). At  $L = 100$  km there is only one peak in surface roughness for the crater due to the crater cavity itself.

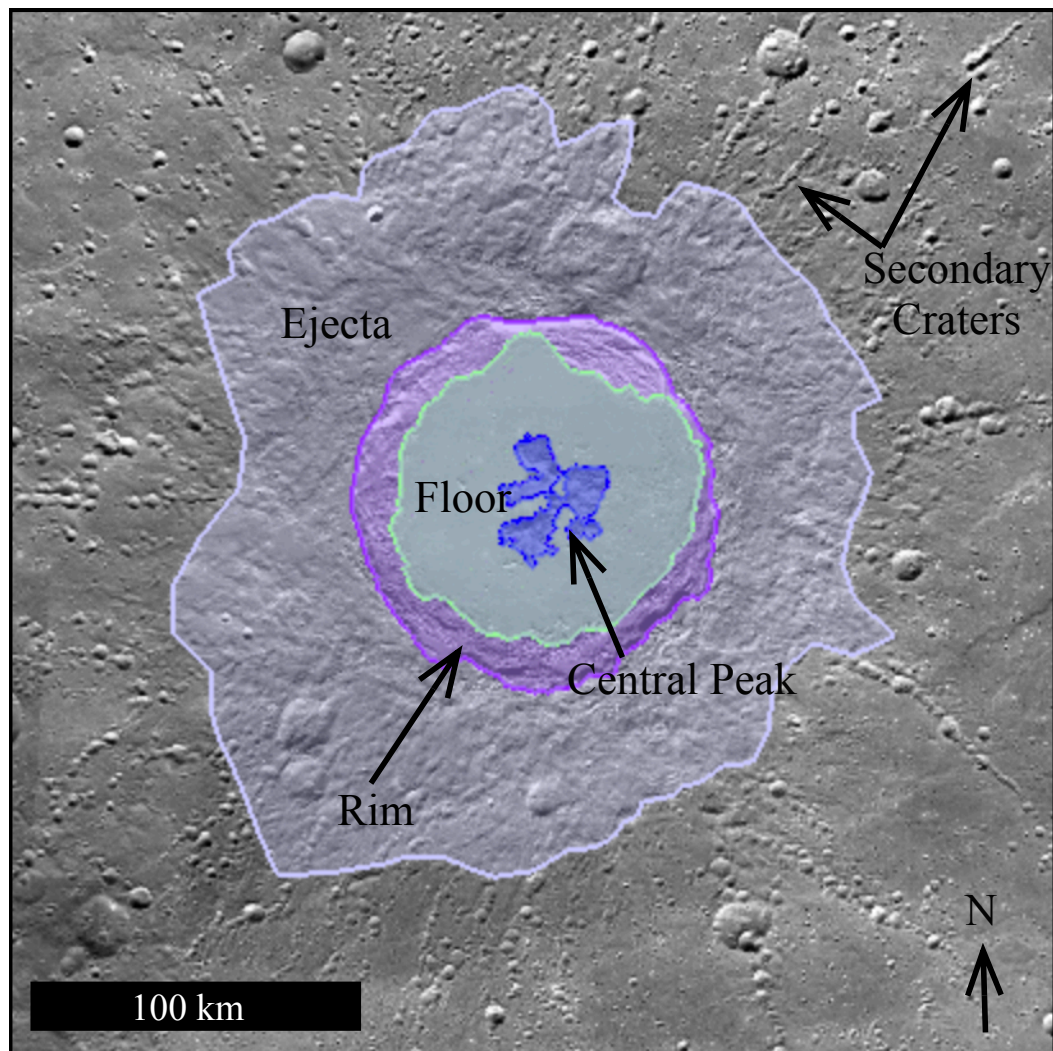


**Figure 5.** A geologic map of the crater Abedin. The ejecta, rim, central peak and crater floor are labeled. A few secondary craters are also identified. This map was used to guide identification of the source of the qualitative local maximum in Fig. 6.

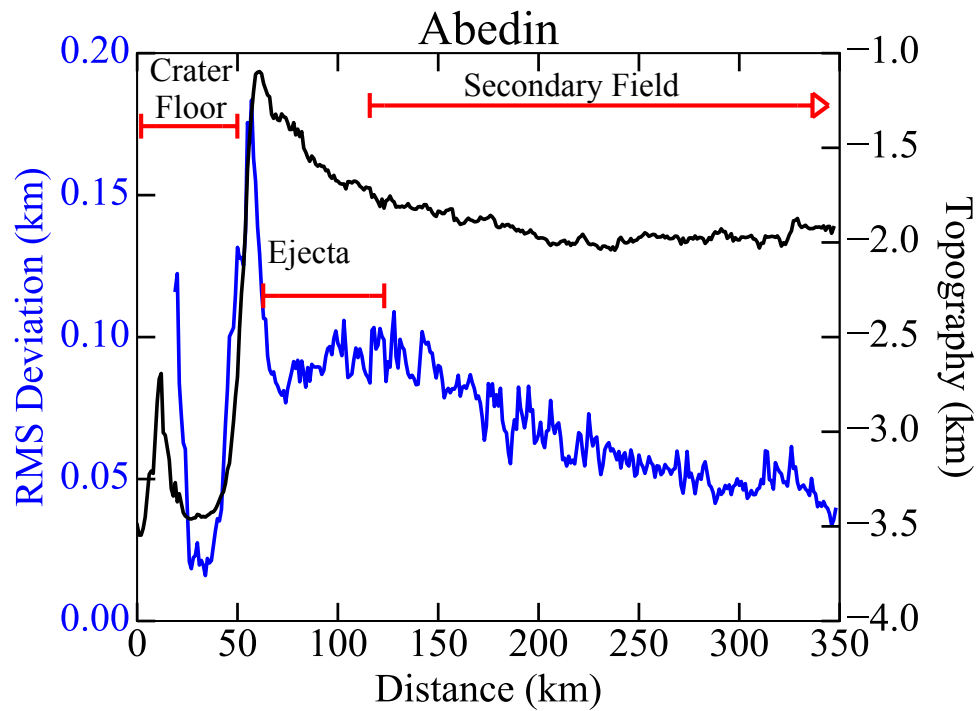


**Figure 6.** The RMS deviation at  $L = 1$  km and MLA topography plotted radially from the center of the crater Abedin (same as Fig. 2(a)) with the radial range of the crater cavity, ejecta, and secondary fields identified.

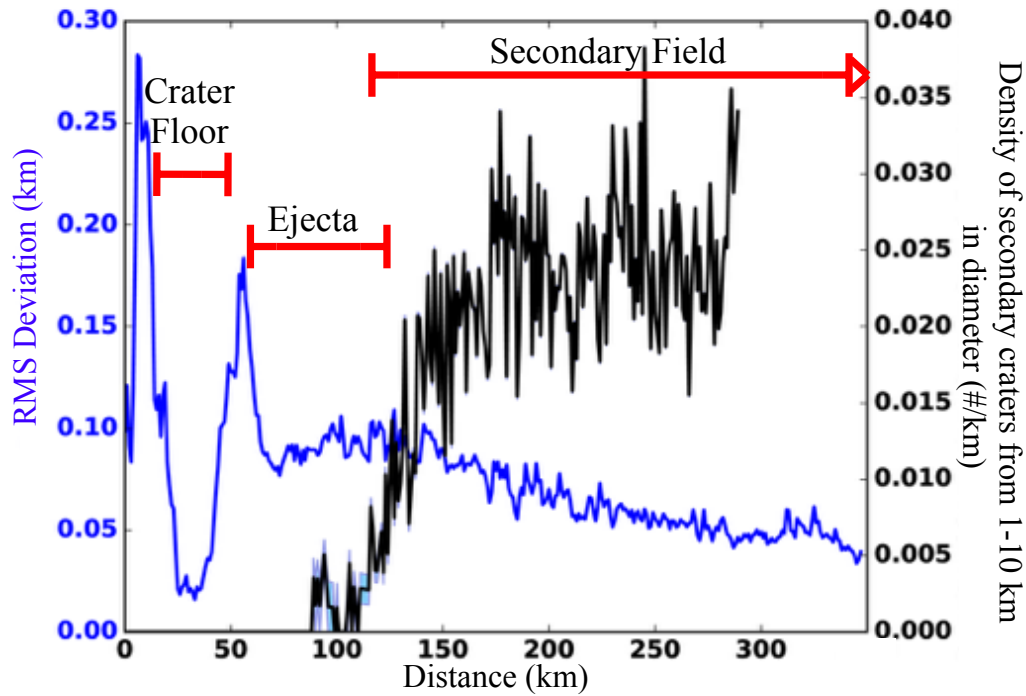


**Figure 7.** Radial surface roughness distribution for Abedin and the radial density distribution of secondary craters ranging in diameter from 1-10 km. The secondary crater density is truncated at a distance of 290 km away from the crater center since we were investigating the qualitative local maximum, which is closer to the crater center. The blue region represents a 1 sigma error bar. The radial mapped distance of the crater floor, ejecta, and secondary fields from Fig. 5 are added for reference.

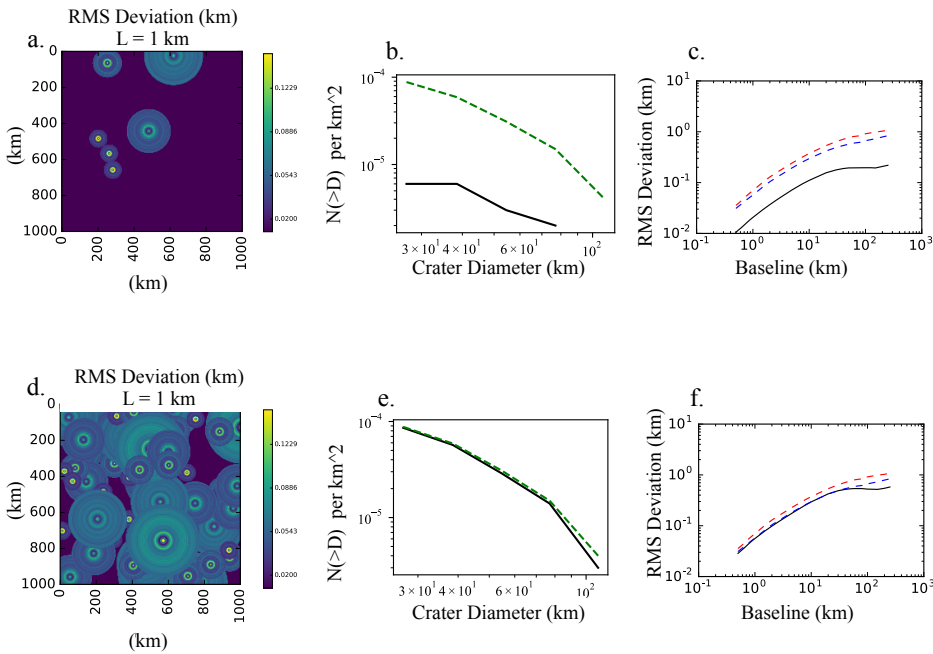


**Figure 8.** (a)-(c) Computed surface roughness obtained after 6 impact craters with diameters ranging from 25 to 120 km are emplaced on a 1000-km-by-1000-km surface where the initial surface roughness is set to zero. (d)-(f) is the same surface with 88 craters emplaced, this matches the size frequency distribution of impact craters with diameters between 25 and 120 km in a 1000-km-by-1000-km area for the cratered terrain [Ostrach *et al.*, 2015]. Maps of the surface roughness are shown in (a) and (d), while (b) and (e) show the number of craters per unit area at this point in the simulation (the black line is the target size-frequency distribution). Deviograms (c) and (f) show the calculated surface roughness of the entire 1000-km-by-1000-km region and can be compared to the observed surface roughness of the cratered terrain (red dashed) and smooth plains (blue dash) *Susorney et al.* [2017].

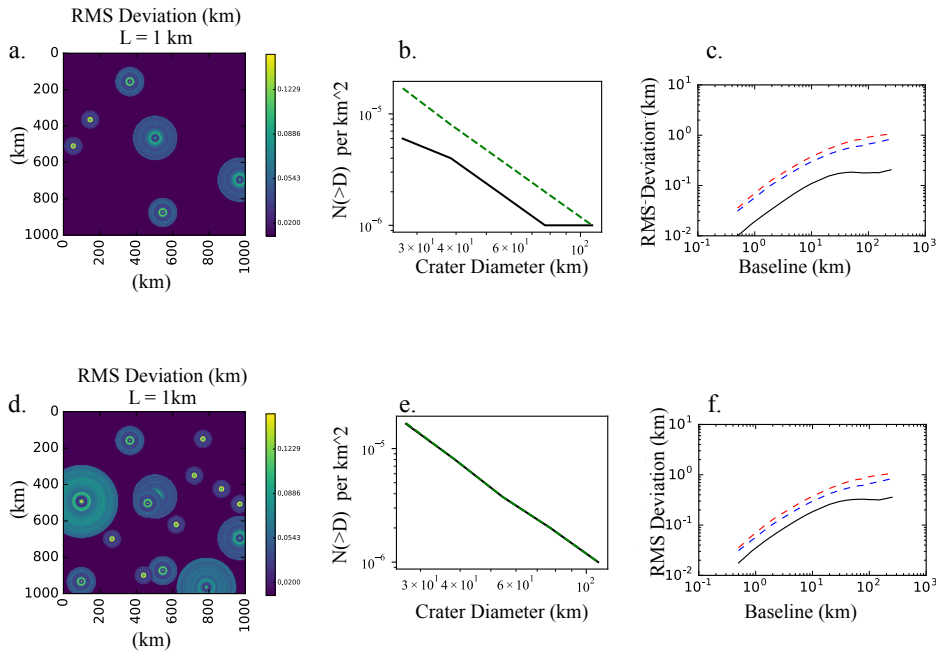


**Figure 9.** (a)-(c) Computed surface roughness obtained after 6 impact craters with crater diameters ranging from 25 to 120 km are emplaced on a 1000-km-by-1000-km surface where the initial surface roughness is set to zero. (d)-(f) is the same surface with 16 craters emplaced, this matches the size frequency distribution of impact craters with diameters between 25 and 120 km in a 1000-km-by-1000-km area for the smooth plains [Ostrach *et al.*, 2015]. Maps of the surface roughness are shown in (a) and (d), while (b) and (e) show the number of craters per unit area at this point in the simulation (the black line is the target size-frequency distribution). Deviograms (c) and (f) show the calculated surface roughness of the entire 1000-km-by-1000-km region and can be compared to the observed surface roughness of the cratered terrain (red dashed) and smooth plains (blue dash) *Susorney et al.* [2017].



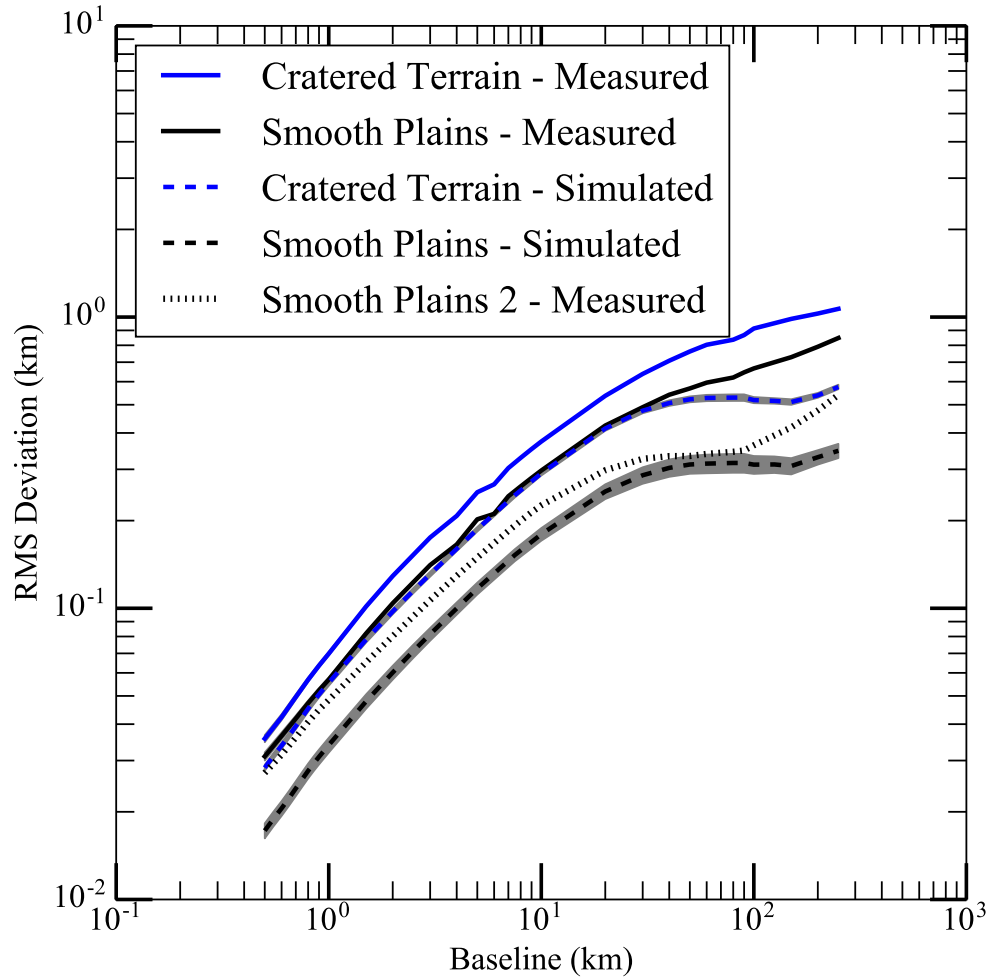


**Figure 10.** A devioqram of the measured [*Susorney et al.*, 2017] and simulated surface roughness for both the smooth plains and cratered terrains on Mercury. Uncertainties associated with the measured surface roughness are from the error of MLA measurements ( $<1$  m) and are smaller than the thickness of the lines plotted. The mean simulated surface roughness of smooth plains and cratered terrains from 30 runs is plotted with a solid line. The gray shaded region represents the one standard deviation of the range of results obtained after 30 runs.

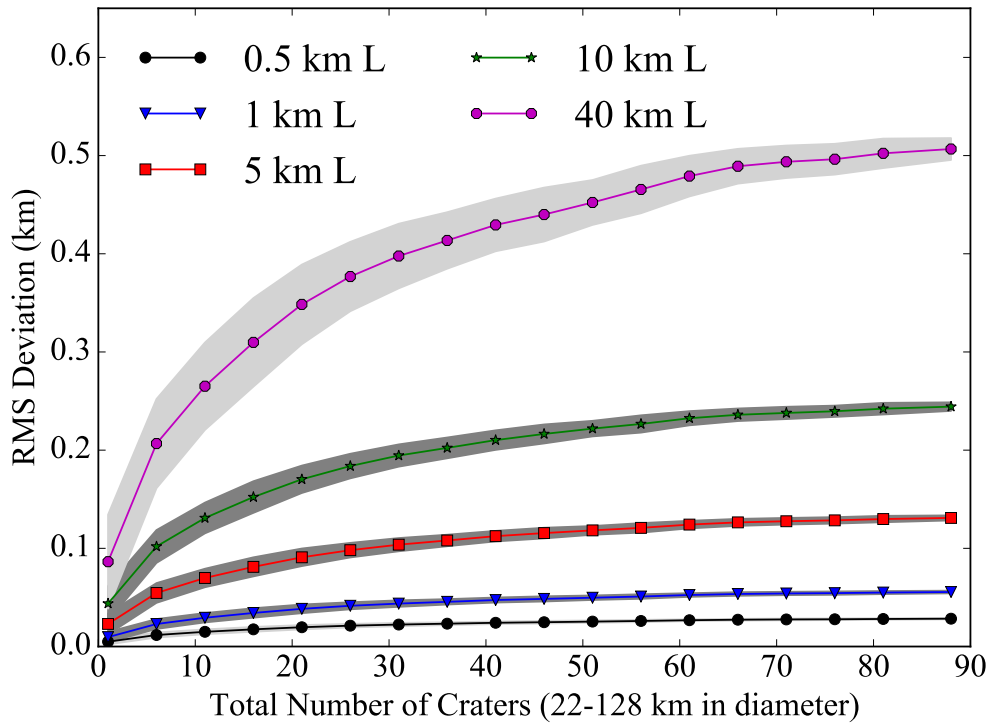


**Figure 11.** RMS deviation (or surface roughness) measured at five baselines ( $L$ ) computed from the numerical investigation as a function of the total number of craters used in the computation (each point represents five additional craters emplaced in the investigation). The gray region is the one standard deviation for 30 runs employed. These simulations were run until surface roughness steady-state was reached.

**Table 1.** Characteristics of the five craters used in the numerical investigation. The freshness classification is scaled 1 - 5, with 5 being the freshest [e.g., *Trask and Guest, 1975*]. The frequency columns are the values from [*Ostrach et al., 2015*] for the size bin each crater is represented in our model and SP refers to the smooth plains and CT refers to the Cratered Terrain.

Crater Name	Diameter (km)	Longitude ( $^{\circ}$ W)	Latitude ( $^{\circ}$ N)	Freshness Classification	Frequency for SP	Frequency for CT
Egonu	25.0	298.5	67.1	4	$1.70 \times 10^{-5}$	$9.16 \times 10^{-5}$
Rivera	40.0	327.8	69.3	4	$8.23 \times 10^{-6}$	$6.27 \times 10^{-5}$
Tung Yuan	60.5	62.8	75.0	3	$3.94 \times 10^{-6}$	$3.49 \times 10^{-5}$
Gaudi	81.0	290.8	76.9	3	$2.15 \times 10^{-6}$	$1.88 \times 10^{-5}$
Stieglitz	100	292.4	72.5	4	$1.07 \times 10^{-6}$	$7.36 \times 10^{-6}$